Algorithmically Controlled Electroporation: A Technique for Closed Loop Temperature Regulated Pulsed Electric Field Cancer Ablation

Ross Aaron Petrella *, Christopher C. Fesmire *, Jacob D. Kaufman, Nomi Topasna, and Michael B. Sano

Abstract*—*Objective: **To evaluate the effect of a closed-loop temperature based feedback algorithm on ablative outcomes for pulsed electric field treatments.** ***Methods:*** **A 3D tumor model of glioblastoma was used to assess the impact of 2 μs duration bipolar waveforms on viability following exposure to open and closed-loop protocols. Closed-loop treatments evaluated transient temperature increases of 5, 10, 15, or 22 °C above baseline.** ***Results:*** **The temperature controlled ablation diameters were conditionally different than the open-loop treatments and closed-loop treatments generally produced smaller ablations. Closed-loop control enabled the investigation of treatments with steady state 42 °C hyperthermic conditions which were not feasible without active feedback. Baseline closed-loop treatments at 20 °C resulted in ablations measuring 9.9 $\pm$ 0.3 mm in diameter while 37 °C treatments were 20% larger ($p < 0.0001$) measuring 11.8 $\pm$ 0.3 mm indicating that this protocol induces a thermally mediated biological response.** ***Conclusion:*** **A closed-loop control algorithm which modulated the delay between successive pulse waveforms to achieve stable target temperatures was demonstrated. Algorithmic control enabled the evaluation of specific treatment parameters at physiological temperatures not possible with open-loop systems due to excessive Joule heating.** ***Significance:*** **Irreversible electroporation is generally considered to be a non-thermal ablation modality and temperature monitoring is not part of the standard clinical practice. The results of this study indicate ablative outcomes due to exposure to pulses on the order of one microsecond may be thermally mediated and dependent on local tissue temperatures. The results of this study set the foundation for experiments in vivo utilizing temperature control algorithms.**

***Index Terms*—Non-thermal high frequency irreversible electroporation, electro-thermal therapy, pulsed electric field, bioelectric, electroporation.**

Manuscript received July 25, 2019; revised October 17, 2019 and November 15, 2019; accepted November 15, 2019. Date of publication May 15, 2020; date of current version July 17, 2020. This work was supported via the provisioning of startup funding from the UNC/NCSU Joint Department of Biomedical Engineering. *(* Ross Aaron Petrella and Christopher C. Fesmire contributed equally to this work.) (Corresponding author: Michael B. Sano.)*

R. A. Petrella, C. C. Fesmire, J. D. Kaufman, and N. Topasna are with the UNC/NCSU Joint Department of Biomedical Engineering.

M. B. Sano is with the UNC/NCSU Joint Department of Biomedical Engineering, Raleigh, NC 27695 USA (e-mail: mikesano@unc.edu).

Digital Object Identifier 10.1109/TBME.2019.2956537

I. Introduction

IRREVERSIBLE electroporation is a tumor ablation technique which utilizes high voltage pulsed electric fields to destroy tumors [1]. While these procedures are generally considered non-thermal [1]–[6], the non-thermal designation only refers to the mechanism of cell death, being the cell membrane phospholipid bilayer reorientation in response to the electric field and the formation of cytotoxic aqueous pores which traverse the cell membrane [2]–[7]. In practice, some of the electrical energy which is applied to the cells or tissue is lost in the form of heat described by Joule heating [8], [9].

Joule heating adds confounding variables to any irreversible electroporation treatment as heat is known to change the biophysical response of cells. For example, when hyperthermia is maintained for extended periods of time proteins begin to denature [10]. Electrically, there are temperature dependent spatiotemporal changes in cell media [11] and tissue conductivity [9], [12] leading to a dynamic reduction in resistance which may need to be accounted for in pulsed electric field treatment planning [13]. For in vitro experiments, elevated temperatures will cause collagen to denature at temperatures above approximately 42 °C. This limitation can make investigating the combinatorial effects of pulsed fields and hyperthermic temperatures challenging in 3D tumor models where the melting point of the matrix is less than the applied Joule heating.

While the heating effects in irreversible electroporation could be minimalized by reducing the pulse repetition rate or decreasing the width of the pulses, this has not been the standard practice [14]. Previous irreversible electroporation protocols have been prescribed in terms of pulse number, amplitude, and repetition rate in order to achieve a targeted treatment energy dose [15]. Temperature is allowed to increase unregulated throughout the duration of the treatment. Although, side effects are rare for irreversible electroporation treatments, uncontrolled elevated temperatures may been a contributing factor to adverse side effects such as coagulative necrosis [16], thrombosis [17], and fistulas [18].

Uncontrolled protocols could be characterized as open loop, being devoid of a feedback mechanism dependent on a process output. The closed loop, thermally controlled, pulsed electric

field ablation technique defined here as algorithmically controlled electroporation (ACE) uses temperature feedback in order to dynamically adjust the pulse delivery rate. ACE uses a set of process inputs (voltage, maximum temperature, and maximum pulse delivery rate) to find an ideal pulse delivery rate which establishes a steady state temperature. The location of temperature sensing could be anywhere throughout the intended ablation volume. In vivo temperature sensors could be used either at the electrode or distal to the electrode in order to protect critical structures such as blood vessels or bile ducts from thermal injury.

In the presented study, the feasibility of ACE as a focal ablation modality is reported. Experiments were conducted to validate both the operation of the temperature control software and investigate the cytotoxic effects of pulsed electric fields delivered with respect to a temperature control algorithm. The basis of this temperature control paradigm was a proportionate control algorithm which adjusts the rate of pulse delivery depending on the difference between a measured temperature and a target temperature value. Pulses are delivered algorithmically until a target total pulse on time or integrated energized time (IET) [19], [20] is achieved. When combined with a pulsed power supply an ACE system was demonstrated for 500 V, 750 V and 1000 V treatments. Without thermal control temperature increases of 5.3 ± 0.3 °C, 11.4 ± 0.7 °C, and 22.0 ± 4.7 °C were observed from a baseline of 20 °C respectively. With temperature control enabled and a target temperature of 25 °C, 24.5 ± 0.5 °C was achieved for 1000 V treatments with similar results observed for lower voltage treatments. Biological experiments indicated that ACE is capable of achieving treatment zones similar to those created with non-temperature controlled irreversible electroporation. The results highlight the thermal dependence of cell death for pulses with durations on the order of 2 μs which has not been observed in non-thermal irreversible electroporation clinical protocols utilizing longer pulse lengths (50–100 μs). The findings from this study set the foundation for in vivo experiments utilizing a temperature controlled pulse delivery rate.

II. Methods

A. Experimental Temperature Control Algorithm

The ACE algorithm has been designed to dynamically adjust the rate of pulse delivery to achieve and maintain a target temperature. The aim is for the temperature to rapidly increase according to a user defined maximum delivery rate (R_{max}) and then decrement to a steady state delivery rate where the targeted temperature is maintained. The rate specifies the amount of pulse on time compared to the total treatment time of an individual pulse sequence. For a biphasic pulse sequence the R_{max} pulse delivery rate is given by:

$$R_{\max} = \frac{\tau_p + \tau_n}{\delta}\left[\frac{\mu s}{s}\right] \tag{1}$$

where τ_p is the pulse width of the positive phase of the delivered pulse, τ_n is pulse width of the negative phase of the delivered pulse, and δ is the temporal delay between pulse sequences. This rate calculation assumes an idea square wave pulse.

After sampling the temperature, T, the instantaneous rate of pulse delivery as a function of temperature, R(T), is calculated as a fraction of R_{max} by an adjustment equation, ρ(T), according to a discretized Heaviside step function (Fig. 1a). The implementation of this done according the following governing equations:

$$R(T) = \rho(\mathrm{T}) \cdot \mathrm{R}_{\max}\left[\frac{\mu s}{s}\right] \tag{2}$$

$$\rho(\mathrm{T}) = 0.5 - 0.9375 \cdot \Gamma(T) + 0.625\Gamma \cdot (T)^3 - 0.1875 \cdot \Gamma(T)^5 \tag{3}$$

$$\Gamma(T) = \frac{(T - T_{\mathrm{target}})}{\beta} \tag{4}$$

$$\beta = T_{\mathrm{target}} \cdot \omega \tag{5}$$

where T is the measured temperature, T_{target} is the user defined temperature set point, and β is the gain adjustment expression where ω is the coefficient affecting the slope between maximum and minimum pulse delivery rate (Fig. 1b). The ω was held constant at 0.5 for all experiments in this study, but can be adjusted to modulate the rate at which the target temperature is achieved.

Waveforms consisting of 2 μs bipolar pulses (Fig. 1c) were delivered according to this algorithm until a user specified dose was achieved. The dose was defined by the integrated energized time (IET) which is calculated by summing the pulse widths of all applied pulses and was calculated as:

$$IET = \sum_{0}^{N} \tau_p + \tau_n \,[s] \tag{6}$$

where N is the number of applied biphasic waveforms. Previous experiments have utilized IET as a metric for dosing as a simplified approach for comparing treatments across a wide spectrum of pulse widths [20]. On this basis, 0.01 s IET was used for all in vitro experiments to approximate doses utilized in typical clinical pulsed electric field procedures [16] and in vitro experiments [20] which delivered 90–100x monopolar pulses or bipolar bursts with durations of 100 μs ($100 \times 100\ \mu s = 0.01$ s).

The previous equations were implemented in software, via a custom Python application which was used to control the pulse generator. A process flow chart describing the implementation can be seen in Fig. 2. In operation, the user specifies the max temperature (T_{max}) and treatment IET (IET_{max}). Using a temperature sensor the instantaneous temperature at the center of the treatment zone is read. The IET of the administered dose is then determined by summing the durations of all previously administered pulses (6). If the IET is greater than or equal to IET_{max} the treatment is completed. Otherwise, the instantaneous temperature is used to calculate the energy delivery rate (2–5). Pulses are then applied according to the calculated rate. Upon completion of the pulse delivery, the IET is incremented and the temperature is rechecked restarting the feedback loop.

B. Algorithmically Controlled Electroporation System

The temperature control algorithm was integrated with a pulse power supply and temperature sensor to create an

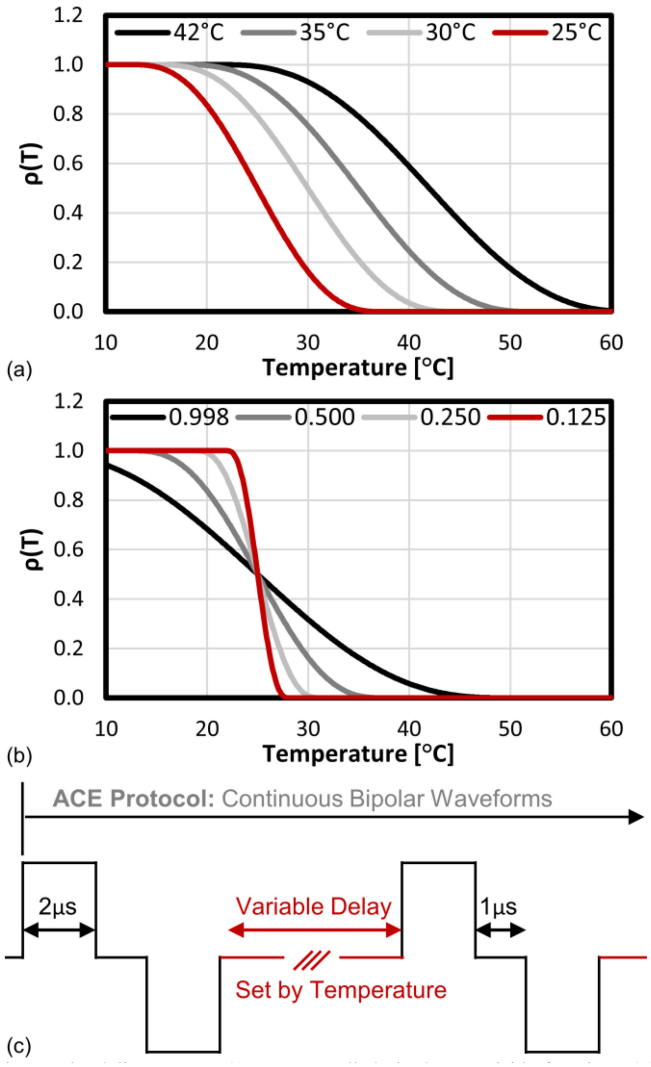

Fig. 1. The delivery rate R(t) was controlled via the Heaviside function ρ(T) which was dependent on the instantaneous temperature (T) measured inside the center pin electrode. (a) The experimental values for ρ(T) are shown for target temperatures (T_{target}) of 25 °C, 30 °C, 35 °C and 42 °C as a function of instantaneous temperatures (T) between 10 and 60 °C. (b) The choice of value for the parameter ω affects the behavior of ρ(T) by modulating how aggressively the algorithm approaches the target temperature. Values in (b) are shown for a target temperature (T_{target}) of 25 °C and ω values of 0.125, 0.25, 0.5, and 0.998. A value of $\omega = 0.5$ was implemented in all experiments. (c) The ACE protocol used in this study delivered bipolar 2 μs pulses with a 1 μs delay between polarity changes. The algorithm adjusts the inter-waveform delay as a function of temperature.

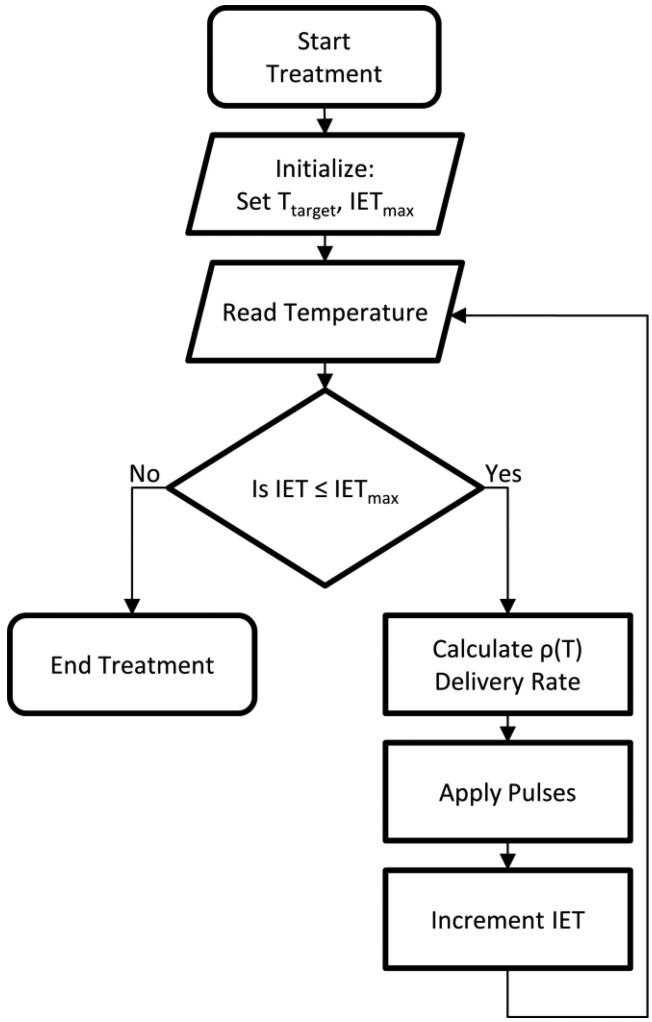

Fig. 2. Algorithm flow chart depicting the method of temperature control by adjustment of the pulse delivery rate. When the temperature is less than the target temperature the maximum delivery rate is set by the user. In the event that the temperature is higher than the T_{target}, the rate of pulse delivery is decreased. A steady state temperature is established when the delivery rate is constant.

algorithmically controlled electroporation (ACE) system. The supply's voltage and current transients have previously been verified both in vitro [20]–[23] and in ex vivo tissue [19], [24], [25]. Briefly, the electronics system used in the experiments was a solid state switched square wave generator with a 20 μF capacitor bank [20], [24]. Biphasic pulses were created using an H-bridge topology. The load was a coaxial or ring-and-pin electrode (Fig. 3a) which has previously been modeled using a finite element model and validated in vitro [20], [21]. The outer ring (Fig. 3a) was fabricated from 19 mm outer diameter 0.89 mm thick 316 stainless steel tubing (89785K259, McMaster-Carr, Douglasville, GA). The inner pin (Fig. 3a) was fabricated from a 1.64 mm outer diameter blunt 304 stainless steel dispensing needle (75165A552, McMaster-Carr, Douglasville, GA). The ring and pin assembly was held in place using a friction fit to a custom laser cut acrylic holder and an electrical connection to the outer ring was made via a friction fit to a 1.64 mm outer diameter blunt 304 stainless steel dispensing needle. The entire assembly was designed to hold the electrodes flush against the bottom at the center of the 12 well plate (Fig. 3b).

Temperature was monitored using an electro-optic temperature probe with an accuracy of ±0.2 °C (TS5, Micronor Inc., Camarillo, CA) placed inside the center conductor of the electrode's inner pin. Temperatures were acquired by a signal conditioner (Fotemp, Micronor Inc., Camarillo, CA) and recorded at 3 Hz. Occasional artifacts from communications errors between

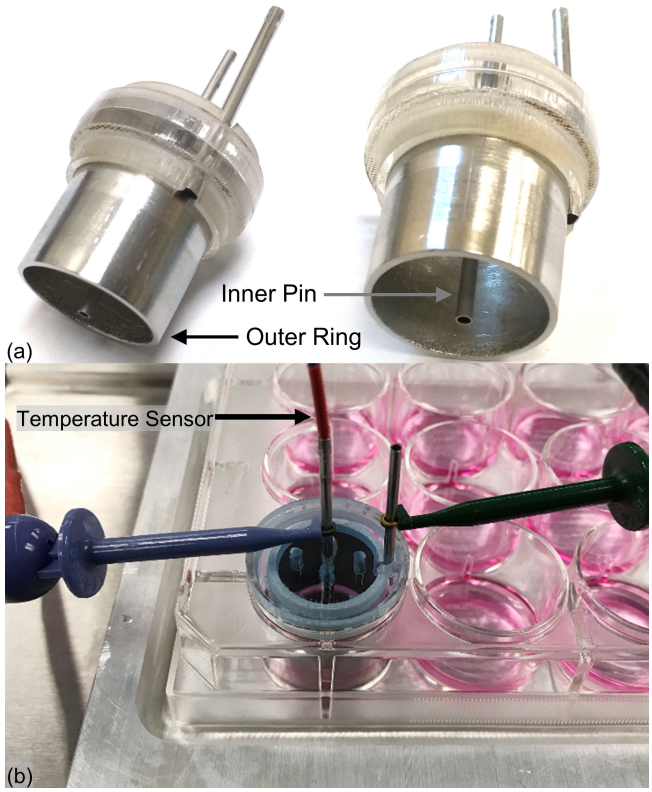

Fig. 3. The coaxial electrode (a) consists of a stainless steel outer conductor, hollow inner conductor, and a laser cut acrylic securing ring. The complete experimental setup is shown in (b). The coaxial electrode is inserted into a single well of a 12-well culture dish and the fiber optic temperature sensor is inserted into the center electrode. Test leads make the electrical connection to the pulse generator.

the signal conditioner and the pulse generator were removed in post-processing. Refinements to the system to improve EMI management ultimately rendered error correction obsolete.

C. Validation of ACE Temperature Control

To validate the operation of the combined temperature control algorithm and pulsed power supply, a probing of the spatial temperature distribution was conducted. To perform this, the temperature sensor was placed inside the hollow center conductor of the coaxial electrode. To the electrode one of three pulse sequences were applied. The basis of all three pulsed power treatments was a biphasic waveform with a transient consisting of a 2 μs positive phase, 1 μs delay, and a 2 μs negative phase, referred to here as a 2-1-2 waveform.

First, a continuous high frequency irreversible electroporation (CH-FIRE, Supplemental Fig. 1a) treatment, which has previously been used in vitro without temperature control [20], was conducted. The treatment protocol for this was 2-1-2 waveforms delivered 2500x with a repetition rate of 25 Hz (e.g., R(T) = 100 μs/s). This treatment had an integrated energized time of 0.01 s (e.g., 2500 $\times$ 4 μs = 0.01 s). Next, a burst high frequency electroporation (BH-FIRE, Supplemental Fig. 1b) treatment, which has been demonstrated in vitro [20], [26] and in vivo [27], [28], was conducted. This consisted of rapidly delivered 2-1-2 waveforms repeated 25x to create a 100 μs burst which was repeated 100x with a repetition rate of 1 Hz (e.g., R(T) = 100 μs/s, IET = 100 $\times$ 100 μs = 0.01 s). Finally, for the ACE treatment a total of 2500x 2-1-2 waveforms were applied with the delivery rate being adjusted by the algorithm (Fig. 1c). For the algorithm inputs R_{max} was 200 μs/s and the target temperature (T_{target}) was 25 °C. To investigate the effects of applied voltage on the control algorithm's behavior and biological outcomes, each of these three treatment regimens were investigated with applied voltages of 500 V, 750 V, and 1000 V with an initial baseline temperature of 20 °C.

To investigate the effects of target temperature (T_{target}) on biological outcomes a series of ACE experiments were conducted (0.01 s IET, 1000 V, 2-1-2 waveforms) with an initial baseline temperature of 20 °C and target temperatures (T_{target}) of 25 °C, 30 °C, 35 °C, and 42 °C. This maximum temperature was chosen to prevent melting of the collagen hydrogels, which occurs at approximately 43–45 °C, from confounding the results.

To investigate the effects of baseline temperature on biological outcomes ACE experiments were conducted (0.01 s IET, 1000 V, 2-1-2 waveforms) with an initial temperature of 37 °C and a target temperature (T_{target}) of 42 °C. Matched uncontrolled, open loop CH-FIRE treatments (0.01 s IET, 1000 V, 2-1-2 waveform, 100 μs/s) resulted in abrupt melting of the collagen hydrogels (Supplemental Fig. 2). This experimental setup had previously been tuned to achieve an approximate 5 °C temperature rise when 500 V treatments were administered at a rate of 100 μs/s [20] which was additionally re-validated here for CH-FIRE, BH-FIRE, and ACE treatments starting at 20 °C and 37 °C (Supplemental Fig. 3).

As a matter of experimental consistency, the volume of the collagen hydrogel and supplemental media were fixed to 500 μL and 100 μL, respectively, in the experiments as described below. However, an additional experimental group was conducted with 1000 μL of supplemental cell culture media to investigate how elevated treatment currents and resulting increased rate of Joule heating affected the ability of the algorithm to maintain adequate temperature stability (Supplemental Fig. 4). All experiments were conducted a minimum of three (N = 3) times and data is presented as mean $\pm$ standard deviation.

Finally, it was of interest to determine how the temperature varied spatially within the region around the electrode to supplement data generated in numerical simulations (see Supplemental Methods**,** Supplemental Fig. 5). In a subset of experiments, with the center pin acting as the temperature control sensor, three additional temperature sensors were used to simultaneously record data at locations approximately corresponding to the radius of observed treatment zones (2.5 mm, 4.0 mm, 5.5 mm). The use of these additional sensors slowed the hardware data sampling rate to 2Hz resulting in less granular data and was therefore not used for the majority of experiments.

D. Cell Culture

Treatment of brain tumors with irreversible electroporation is of interest and is representative of an irreversible electroporation application where precise control over thermal

conditions is desirable [6], [29], [30]. Grade IV human glioblastoma cells (U118, HTB-15, ATCC Inc., Manassas, VA) were cultured in a complete media consisting of Dulbecco's Modified Eagle Medium (DMEM)(11965118, Gibco, Gaithersburg, MD), supplemented with 10% V/V Fetal Bovine Serum (A3160601, Gibco, Gaithersburg, MD) and 2% V/V Penicillin-Streptomycin solution (15070063, Gibco, Gaithersburg, MD) until reaching approximately 80% confluence. The cells were then harvested via trypsinization (25200056, Gibco, Gaithersburg, MD), centrifuged, and suspended in media at a concentration of 1×10^6 cells/mL. The cells were suspended at a 1:1 ratio in complete cell culture media and PureCol EZ gel (5074-35ML, Advanced Biomatrix, San Diego, CA) with a final cell density of 5×10^5 cells/mL. 500 μL of the mixture was transferred into each well of a 12-well plates (Fig. 3b) to create a 3D culture model approximately 2 mm in height. The mixture was then be incubated for 24 hours at 37 °C to allow the collagen to solidify and for the cells to stretch out, resulting in a more physiological morphology of the cells. The collagen scaffolds were incubated with 500 μL of additional media before and after treatments. However, immediately before treatments the volume was reduced to 100 μL to ensure a consistent electrical resistance between experiments.

E. In Vitro Evaluation of ACE Ablation Geometry

Finally, it was of interest to determine whether closed loop temperature controlled treatments with a dynamic pulse delivery rate produces different sized ablations than a standard open loop treatment. To test this the 3D cell culture model was used with the ring-and-pin electrode. The three pulse protocols which were described in the temperature control verification section were then applied to the well plate. For all cell experiments, the starting temperature was 20 °C. In ACE treatments the target temperature was 25 °C.

Following treatment, the cells were incubated for 24 hours. Each well was then stained with 2 μL of 4 μM Calcein AM (C3100MP, Invitrogen, Carlsbad, CA) to identify viable cells (green) and 50 μL of 100 mg/mL propidium iodide (0219545825, MP Biomedicals, Santa Ana, CA) to identify dead cells (red). A Leica DMi8 microscope with a 4.2 megapixel digital camera (DFC9000GT, Leica Inc., Wetzlar, Germany) was used to capture images at 1.25x and 2.5x which were stitched together using the microscope's software (LASX, Leica Inc. Wetzlar, Germany). The electrode geometry used produced a circular region of cell death. The diameter was measured horizontally, vertically, and twice diagonally using the microscope's software. This is a technique which is representative of how tumor ablations would be described in vivo. Values from these measurements and calculations are presented as mean $\pm$ standard deviation. Measurements comparing ACE to both CH-FIRE and BH-FIRE were statistically compared using a two sample t-test assuming equal variance at a significance level of $\alpha = 0.05$.

Computational simulations of the experimental protocol were conducted to evaluate the heat distribution throughout the 3D tumor model using the Heat Transfer and Electric Currents modules in COMSOL Multiphysics (V5.3, COMSOL Inc., Los Altos, CA). A complete accounting of these methods can be found in the supplemental materials.

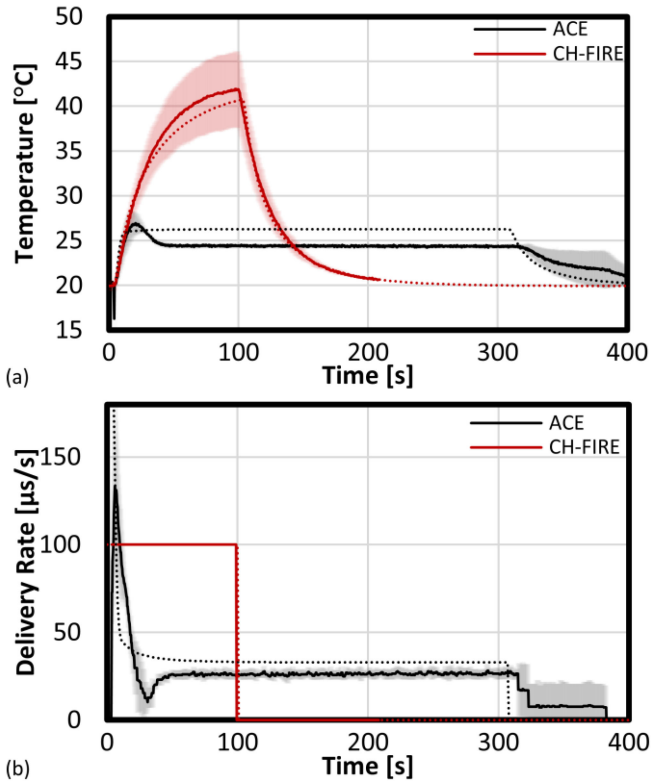

Fig. 4. Temperature transients and delivery rates for 1000 V 0.01 s IET treatments with initial temperatures of 20 °C. (a) ACE treatments (black) have a lower peak temperature but longer treatment times than uncontrolled (red) CH-FIRE treatments. (b) In ACE the dynamic energy delivery rates are automatically adjusted (black) to maintain the desired treatment temperature throughout the treatments. In contrast, CH-FIRE treatments have a single energy delivery rate (100 μs/s) throughout the treatment. Solid lines represent mean experimentally measured temperatures, dotted lines represent simulated temperatures, and shaded areas represent one standard deviation from the mean.

III. Results

A. Validation of the Algorithm

To validate the operation of the ACE algorithm and system, two initial starting temperatures with two T_{target} levels were evaluated. These outcomes were then compared to a non-temperature controlled CH-FIRE and BH-FIRE treatment. For ACE, the results show that the treatment was successful at elevating the temperature to a set T_{target} and maintaining the temperature for the duration of the treatment. The temperature transient (Fig. 4a) shows that for a programmed 5 °C increase, the temperature reaches the intended T_{target} after approximately 11 s of energy delivery.

For both ACE and CH-FIRE the profile of the temperature increase was approximately exponential. After the initial temperature increase in ACE, the temperature waveform had a flat top with an average temperature of 24.4 $\pm$ 0.3 °C for the T_{target} = 25 °C treatment. In contrast, the matching CH-FIRE

treatment reached a peak temperature of 42.0 ± 4.2 °C. These treatments were completed after 340.1 ± 36.9 s and 100.0 ± 0.0 s respectively.

These temperature results are mirrored in the temporal development of the pulse delivery rate (Fig. 4b). Initially in ACE, the pulse delivery rate was set to 200 μs/s. Due to the rapid increase in temperature, there was a reduction in the pulse delivery rate governed by Eqs. 2–5. For the 25 °C treatment the steady state pulse delivery rate was 26.7 ± 7.8 μs/s; whereas, the pulse delivery rate was 100 μs/s for the matched CH-FIRE and BH-FIRE treatments.

An overshoot of approximately 2 °C was observed for 1 kV ACE treatments with a 25 °C temperature set point which was mirrored in the numerical simulations (Fig. 4a). This was accounted for experimentally by incrementally decreasing the energy delivery rate when sustained temperatures above the set point were detected. Overshoot was not observed for 500 V ACE treatments where 0.1 mL of supplemental media was added to the wells (the standard, protocol, Supplemental Figs. 3–4), but was observed in experiments where 1.0 mL of media were present in the wells (Supplemental Fig. 4) indicating that treatment current, rate of heating, treatment load impedance, and temperature set points affect algorithmic performance.

In contrast to ACE treatment, both the CH-FIRE and BH-FIRE treatments had a significant increase in temperature beyond the T_{target} used for ACE with no steady state temperature being reached across the voltage range tested. Temperature increases only stopped when the full IET was delivered and treatment was stopped. Both CH-FIRE and BH-FIRE had a constant pulse delivery rates of 100 μs/s (Fig. 4b).

Outside of the central electrode which was the feedback location used in ACE treatments, the temperature was found to vary spatially (Fig. 5). Points distal to the center electrode were found to have similar temperature transients to the center electrode in that there was a rapid increase in temperature which then reached a steady state value. For the points measured this was 25.0 ± 0.3 °C at 2.5 mm, 22.8 ± 0.2 °C at 4 mm, and 21.1 ± 0.2 °C at 5.5 mm from the treatment center.

The temperature around the center electrode in the 1000 V CH-FIRE treatments were also found to vary spatially reaching mean peak temperatures of 36.6 ± 1.4 °C at 2.5 mm, 30.2 ± 1.3 °C at 4.0 mm, and 25.9 ± 1.1 °C at 5.5 mm from the treatment center.

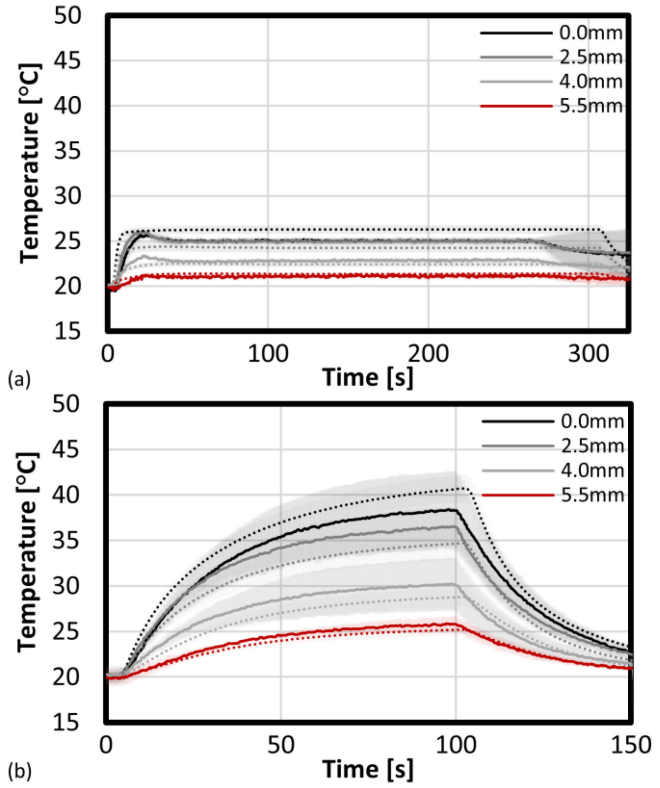

Fig. 5. The temperature around the center electrode decreases radially. (a) In 1 kV ACE treatments there is a rapid increase in temperature to the set point of 25 °C at the center of the coaxial electrode. The temperature increases throughout the gel in a transient manner which mirrors the center electrode. At a radius of 5.5 mm the ACE treatment has a peak temperature of 21.2 °C. (b) In CH-FIRE treatments the temperature increases throughout the 100 s of treatment time. At the center electrode the temperature reached a mean peak of 38.3 °C. The temperature gradient extended outward reaching a temperature of 25.2 °C at a radius of 5.5 mm. Solid lines represent mean experimentally measured temperatures, dotted lines represent simulated temperatures, and shaded areas represent one standard deviation from the mean.

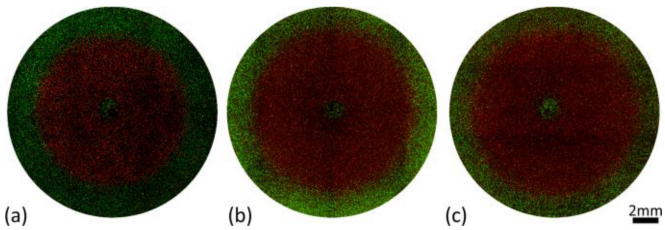

Fig. 6. Microscope images comparing (a) ACE, (b) CH-FIRE, and (c) BH-FIRE ablations following treatment with 1 kV waveforms and an IET of 0.01 s for treatments with a baseline temperature of 20 °C. Cell death is indicated by the red propidium iodide staining and live cells are green due to activated Calcein AM. The presence of live (green) cells in the center of the treatment zones indicate that cells were unaffected by temperature transients and were not exposed to lethal electric fields inside of the hollow pin electrode.

B. Biological Effects Are Conditionally Temperature Dependent

Having established the effectiveness of the combined ACE algorithm and pulse power supply, it was of interest to determine whether ACE would produce different ablations than that of either CH-FIRE or BH-FIRE. Representative fluorescence microscopy images showing ablations of 1 kV, 0.01 s IET treatments with a baseline temperature of 20 °C can be seen in Fig. 6. Generally, the shape of the ablation was circular around the center electrode which is characteristic of the electrode geometry. The margin or transition between live and dead cells was sharp in all three tests and similar to previous ablations using this electrode geometry [20], [21].

Measurements of the ablation diameters were used to indicate the effectiveness of the treatment. For all treatment profiles the ablation diameter was dependent on the applied voltage (Fig. 7). An increase in voltage resulted in a larger ablation. The

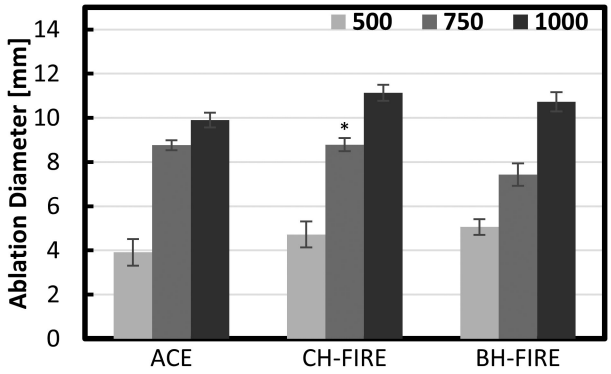

Fig. 7. A comparison of ablation sizes across pulsed electric field schemes at different voltages. The size of the ablation increases with applied voltage. At 500 V ETT ablation diameter was different than H-FIRE and BH-FIRE with ACE producing smaller ablations. At 750 V ACE was equivalent to CH-FIRE and different than BH-FIRE with BH-FIRE being smaller. At 1000 V ETT was different than both H-FIRE and BH-FIRE with ETT having the smaller ablation diameter. The ACE treatments had a 25 °C temperature set point. $*$ indicates treatments which were found to be statistically equivalent to voltage matched ACE treatments ($p = 0.9$).

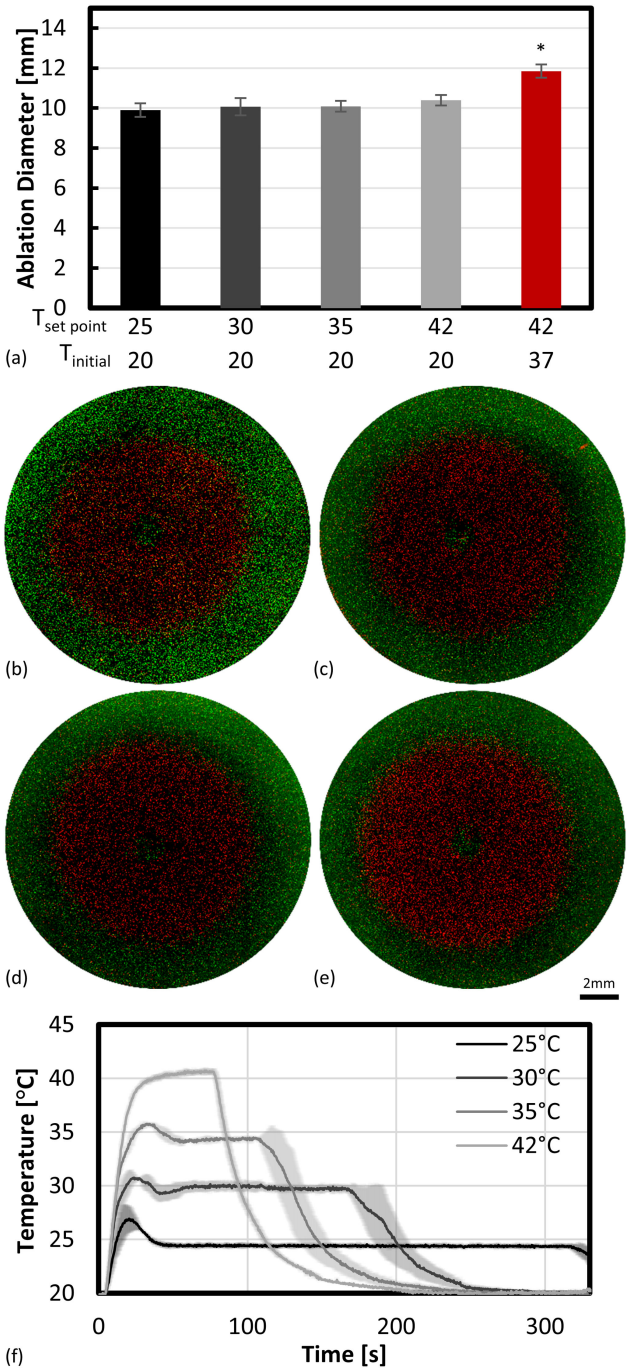

Fig. 8. (a) Ablation diameters as a function of initial temperature ($T_{initial}$) and temperature set point ($T_{setpoint}$). Live (green) and dead (red) staining of 3D tumor mimics treated with 1 kV 0.01 s IET ACE administered with a baseline temperature of 20 °C and temperature set points of (b) 25 °C, (c) 30 °C, (d) 35 °C, and (e) 42 °C. (f) Mean temperature profiles from these treatments where the shaded regions represent one standard deviation. Asterisk indicates significantly significant difference from all 20 °C baseline treatments ($p < 0.0001$).

increase in ablation diameter was non-linear. For example, in ACE treatments there was a rapid increase in ablation diameter from 3.9 mm to 8.8 mm when the voltage was increased from 500 V to 750 V (125% increase). On the other hand, there was only a moderate increase in ablation size from 8.8 mm to 9.9 mm (12.5% increase) when ACE voltage was increased from 750 V to 1000 V. CH-FIRE exhibited a similar dependence on voltage. Between 500 V and 750 V there was 87% increase in ablation diameter. Whereas, between 750 V and 1000 V there was a 26% increase in the ablation diameter. In the tested voltage range BH-FIRE was approximately linear. When comparing 500 V and 1000 V, a doubling in voltage resulted in an approximate doubling of ablation diameter.

Of the protocols comparing ACE, CH-FIRE, and BH-FIRE only two pairs had ablation measurements that were found to be statistically indistinguishable, 500 V BH-FIRE with 500 V CH-FIRE ($p = 0.08$) and 750 V ACE with 750 V CH-FIRE ($p = 0.9$). All other treatment protocol combinations were found to have ablation measurements which were statistically different ($p = 0.0001$–0.03). In summary, five of the six comparisons yielded ACE ablation diameters which statistically different than CH-FIRE and BH-FIRE ($p < 0.0001$). In each of these cases, the ACE treatment zone was smaller than the equivalent CH-FIRE or BH-FIRE treatment.

For 1 kV ACE treatments with an initial temperature of 20 °C (Fig. 8a) the smallest ablations, measuring 9.9 ± 0.3 mm, were created for treatments with a temperature set point of 25 °C (Fig. 8b). Larger ablations were created for treatments with set points of 30 °C (10.1 ± 0.4, Fig. 8c), 35 °C (10.1 ± 0.3, Fig. 8d), and 42 °C (10.4 ± 0.3, Fig. 8e). A statistically significant difference ($p = 0.0003$) was found between the 25 °C and 42 °C temperature set point groups. Analysis of the temperature profiles (Fig. 8f) for these treatments indicated that the 25 °C set point temperature was achieved in 13.2 ± 4.0 s and the algorithm maintained a steady state temperature of 24.4 ± 0.3 °C throughout the remainder of the treatment. The 30 °C set point was reached in 22.44 ± 4.5 s and the steady state temperature was 29.8 ± 0.3 °C. The 35 °C set point was reached in 25.0 ± 2.13 s the steady state temperature was 34.6 ± 0.5 °C. The 42 °C set point was approached, but not achieved prior to the treatment

delivering the prescribed 0.01 s IET dose. In these experiments, the temperature reached 40 °C in an average of 36 ± 5.5 s and had a mean temperature of 40.3 ± 0.2 °C from this time (36 s) until the end of treatment.

ACE treatments with a starting temperature of 37 °C (Supplemental Fig. 2b) were found to be statistically ($p < 0.0001$) larger than any of the ACE treatments conducted with a baseline temperature of 20 °C (Fig. 8a). These 37 °C baseline ACE treatments were also statistically larger than the 1 kV CH-FIRE and BH-FIRE treatments conducted with a baseline temperature of 20 °C (Fig. 7, $p < 0.0001$). Matching 1 kV BH-FIRE and CH-FIRE treatments were attempted at a baseline temperature of 37 °C, however, rapid uncontrolled heating resulted in denaturing and melting of the collagen hydrogels (Supplemental Fig. 2a) preventing direct comparison for these protocols.

When 500 V ACE treatments were conducted with a baseline temperature of 37 °C (Supplemental Fig. 3) the treatment yielded peak temperatures of 42.1 ± 0.5 °C and resulted in ablations measuring 7.0 ± 0.3 mm. Matching CH-FIRE and BH-FIRE treatments yielded peak temperatures of 42.8 ± 0.2 and 43.6 ± 1.1 °C and ablations which were sequentially larger than the matching ACE treatment, measuring 8.3 ± 0.5 mm and 8.9 ± 1.6 mm, respectively.

IV. Discussions

A method for algorithmic control of pulsed electric field delivery rate for tumor ablation has been presented. The technique was designed to restrict temperature rise due to delivery rate associated Joule heating and to maintain a user desired temperature. The operation of both the algorithm and ACE system was validated in vitro against both CH-FIRE and BH-FIRE treatments. The ACE treatment was shown to rapidly increase in temperature due to the elevated R_{max} level (2) of 200 μs/s. This R_{max} is a faster delivery rate than typically used in CH-FIRE and BH-FIRE treatments [23], [26], [30], [31], however, throughout the rising phase of the temperature transient the rate of pulse delivery (Eq. 2, R(T)) was algorithmically decreased. This allowed the temperature to plateau at the user defined set temperature (T_{max}). Ultimately, the software control was able to maintain the temperature within ±0.5 °C.

Although the presented control algorithm was successful in being able to maintain temperature near the set point, modifications to the current algorithm as well as other control algorithms could improve performance. In the current implementation of ACE the control algorithm could be considered a type of proportional controller as the output is proportional to an error signal (2). The signal error, ρ(T), is a function of the difference between a set point and a process variable, in this case the temperature reading. Its operation is dependent on signal error or a difference between the current temperature and the set point temperature in order to generate an output. There are two main limitations to this current setup. First is that proportional band is limited by R_{max}, making negative deviation from T_{target} permanent. If R_{max} was set too low, the target temperature would not be reached before the full IET was delivered. If this was the case the ACE treatment would be the same as a CH-FIRE treatment of the same pulse delivery rate. While not observed in these experiments, another limitation is that the error function could be unable to sufficiently change to meet the process variable. This describes an instance where greater pulse delivery rate is needed for the same temperature error. Conceivably, this could happen in vivo where the ablation is near a major blood vessel or in tumors with significant angiogenesis. Heat sinking as described by the Pennes Bioheat Equation or active electrode cooling could draw away heat causing additional increases in pulse delivery rate to be needed to cause the same increase in temperature. A solution to this potential problem would be to utilize a different control model. Most notably a proportional-integral-derivative (PID) algorithm could be used. The integration term could be used to increase the pulse delivery rate as a function of error and time, negating heat sinking effects. The derivative term could also have the added benefit of reducing overshoot and ripple in the temperature transient.

Future ACE algorithms also have the option of different or multiple controller outputs in order to maintain T_{target}. The presented system used pulse delivery rate as the only controller output, but other pulse properties are known to affect Joule heating. This includes using voltage or pulse width. A combination of dynamic adjustment of pulse delivery rate, voltage, and pulse width is possible and could take advantage of multiple bioelectric phenomena. For example long pulses on the order of 100 μs are known to cause instant cell death by irreversible electroporation but also cause rapid heating [32]. On the other hand, short nanosecond pulsed electric fields are less likely to induce heating and cause cell death by apoptosis [33].

This dynamic adjustment of multiple pulse parameters could also be used to address the discrepancy in treatment time between ACE and CH-FIRE or BH-FIRE. In the current implementation, there is a design tradeoff between throttling the pulse delivery rate and extending the treatment time. Once the temperature has reached a steady state, the voltage could be lowered or the pulse width reduced in order to continue to increment the IET without causing extra heating. However, there are some challenges with dynamically adjusting the applied voltage and pulse widths [32] as each of these parameters are known to significantly affect ablation sizes [19], [20], [27] as reinforced in Fig. 7 and Supplemental Fig. 2. It is also noted that the speed of pulse delivery could be increased by changing the applicator electrode and utilizing a cooled electrode such as that currently used in microwave ablation treatments [34] where chilled saline solution pumped through the hollow applicator electrode acts as a heat sink for the pulses.

In most scenarios the maximum rate of Joule heating will occur adjacent to the electrode-tissue interface where the electric field is at a relative maxima. However, it should be noted that alternative applicator designs may affect the temperature distribution in the surrounding tissue and additional engineering effort may be necessary to acquire temperatures at regions of interest which are suitable for use in the control algorithms. Alternatively, it may be of interest for clinicians to prescribe a certain maximum temperature at a distal location (e.g., in proximity to an adjacent nerve bundle) in which case a distal temperature sensor could be used to acquire the control signal.

The in vitro viability assay indicates that ACE ablation effectiveness with respect to non-temperature controlled CH-FIRE and BH-FIRE is conditional. When controlling for the baseline treatment temperature, ACE generally produced smaller ablations. One explanation of this could be that the lateral propagation of temperature (Supplemental Figs. 5, 6, Fig. 5) has an effect on the cell fate following treatment. In the case of CH-FIRE and BH-FIRE treatments (Fig. 5b) the temperature at the ablation margin (radius = 5.5 mm) reached a temperature of 25.9 ± 1.1 °C which was greater than the ACE center (25.0 ± 0.3 °C) and ACE 5.5 mm (21.1 ± 0.2 °C) temperatures for the matched treatments. This potentially allowed for temperature dependent cell membrane changes to occur locally during treatments, thereby decreasing the electric field required to induce cell death and producing larger ablation sizes.

This hypothesis was further explored via ACE experiments conducted with a baseline temperature of 37 °C (Supplemental Fig. 2) which unilaterally produced larger ablations than all treatments conducted with a 20 °C baseline temperature. 1 kV CH-FIRE and BH-FIRE treatments could not be conducted due to temperatures melting the collagen hydrogels (Supplemental Fig. 1). However, 500 V treatments at 37 °C were conducted. Under these conditions CH-FIRE and BH-FIRE treatments reached sequentially greater temperatures and resulted in correspondingly larger ablations than the matching ACE treatments (Supplemental Fig. 2).

Irreversible electroporation is widely considered to be a non-thermal mechanism of cell death [4]–[6], [35]–[37]. Within this context, most prior in vitro work was conducted at room temperature (approximately 20 °C) [26], [30], [38], [39] rather than at physiological temperatures (37 °C). The results presented here, however, highlight the extent that temperature plays a role in pulsed electric field treatments in the single microsecond pulse duration space and indicates that a novel process for inducing cell death may exist in this regime. The outcome could have been expected as there is a reported synergy between elevated temperature and pulsed electric field ablation efficiency with nanosecond electrical pulses [40], however, apoptotic cell death observed in the nanosecond timeframe generally takes multiple days to manifest while cell death was observed here within 24 hours. Further detailed mechanistic studies will be necessary to delineate the mechanisms of cell death which are occurring for ACE at elevated temperatures verses those observed for irreversible electroporation and nanosecond pulse treatments.

There are several simultaneous factors that are thought to contribute to the observed temperature dependence. One explanation for this phenomenon is differences in the extracellular environment, notably changes in cell culture media conductivity. As there temperature rises there is an increase in conductivity [11], resulting in an increase in current delivered to the cells. This temperature dependent change in media conductivity was not found to substantially affect the electric field distribution within the 3D tumor model (Supplemental Figs. 7, 8) which indicates that the observed larger ablations at 37 °C were not due to a favorable distortion of the electric field and instead tied to thermally mediated bio-electric effects.

The transmembrane potential as described by Nernst [41] is directly proportional to temperature. The increase in transmembrane voltage could sensitize either the membrane itself or voltage sensitive channels to pulsed electric field application. When the temperature is altered there are also physical changes to the phospholipid bilayer [42]. The phospholipids can enter a fluid phase where the tail length is reduced [43]. A reduction in tail length and corresponding membrane thickness could result an increase in cell membrane capacitance modifying the transmembrane potential response to external fields ultimately affecting both cell membrane and intracellular responses [26]. Similarly, changes to the cell membrane thickness may alter the ultimate breakdown strength of the membrane or pore formation dynamics yielding more rapid damage to the cell membrane. Replicating the experiments presented here at a multitude of baseline temperatures with pulses spanning multiple orders of magnitude may further help elucidate the mechanism behind the temperature dependent responses observed here. Uncovering the contribution of these factors as a function of temperature will be the focus of future work.

Outside of temperature dependent biophysical changes that may be occurring, the pulse delivery scheme of ACE could be responsible for differences between CH-FIRE and BH-FIRE. As the amplitude, pulse widths, and overall dose (IET) were the same, the variable factor was the pulse delivery rate, which the ACE algorithm dynamically adjusts. In ACE the initial rate of pulse delivery was much higher than what was in CH-FIRE or BH-FIRE (Fig. 4b). This could indicate that ablation size was not dependent on the initial pulse delivery rate, but may be related to the sustained delivery rate which has been shown to affect membrane permabilization [44]. Another factor which may play is role is treatment time. ACE treatment times in vitro were generally longer due to the need to constrain temperature, however, ACE treatments were faster for 500 V treatments (Supplemental Fig. 2) due to the increased initial delivery rate. These ACE treatments were ultimately also smaller than CH-FIRE and BH-FIRE treatments indicating that treatment time has a limited impact on the observed outcomes. However, this could indicate that ablation diameters are dependent on time above a critical temperature. In the future IET in ACE could be modified to find equivalences of treatment time to study this concept.

Noting that ACE is administered different than both CH-FIRE and BH-FIRE opens up new areas of biophysical investigation. For example, in this experiment T_{target} was held constant throughout the treatment time. The set temperature could be made to change throughout the treatment time. This would introduce thermocycling to pulsed electric field treatments. ACE could also be used to finalize treatments in vivo where a rapid increase in temperature at the end of treatment could be used to prevent tumor reseeding along the insertion path of the electrode.

V. Conclusion

Previous pulsed electric field protocols could be characterized as open loop. Once the pulse voltage, number, and frequency are

set by the user, they are delivered uninterrupted. The presented algorithmically controlled electroporation (ACE) therapy alters this paradigm by dynamically adjusting the pulse delivery rate in order to maintain a target in situ temperature. ACE was validated in vitro via a 3D tumor model. The proportional control algorithm and electronics system were able to establish and maintain a target temperature within 0.5 °C of prescribed target temperatures. A viability assay was conducted and determined that ACE produced different ablation sizes than previous treatment protocols CH-FIRE and BH-FIRE. Generally, the ACE treatments were smaller than CH-FIRE and BH-FIRE. However, some treatments were equivalent in 750 V protocols. ACE enabled the evaluation of protocols at physiological temperatures, which otherwise would not be feasible due to excessive Joule heating. These experiments indicate that electroporation is a thermally mediated effect for pulses on the order of one microsecond. This work sets the foundation for in vivo study of ACE where it is of interest to determine the role of thermal damage as seen in histological differences between ACE and CH-FIRE or BH-FIRE.

REFERENCES

[1] R. V. Davalos *et al.*, "Tissue ablation with irreversible electroporation," *Ann. Biomed. Eng.*, vol. 33, no. 2, pp. 223–231, 2005.

[2] R. V. Davalos *et al.*, "Theoretical analysis of the thermal effects during in vivo tissue electroporation," *Bioelectrochemistry*, vol. 61, no. 1/2, pp. 99–107, 2003.

[3] E. Maor *et al.*, "Non thermal irreversible electroporation: novel technology for vascular smooth muscle cells ablation," *PloS One*, vol. 4, no. 3, 2009, Art. no. e4757.

[4] M. Phillips *et al.*, "Non-thermal irreversible electroporation for tissue decellularization," *J. Biomech. Eng.*, vol. 132, 2010, Art. no. 091003.

[5] C. B. Arena *et al.*, "High-frequency irreversible electroporation (H-FIRE) for non-thermal ablation without muscle contraction," *Biomed. Eng. Online*, vol. 10, no. 1, 2011, Art. no. 102.

[6] P. A. Garcia *et al.*, "Non-thermal irreversible electroporation (N-TIRE) and adjuvant fractionated radiotherapeutic multimodal therapy for intracranial malignant glioma in a canine patient," *Technol. Cancer Res. Treatment*, vol. 10, no. 1, pp. 73–83, Feb. 2011.

[7] T. Kotnik *et al.*, "Membrane electroporation and electropermeabilization: Mechanisms and models," *Annu. Rev. Biophys.*, vol. 48, pp. 63–91, 2019.

[8] I. Lackovic R. Magjarević, and D. Miklavčič, "Three-dimensional finite-element analysis of joule heating in electrochemotherapy and *in vivo* gene electrotransfer," *IEEE Trans. Dielectr. Electr. Insul.*, vol. 16, no. 5, pp. 1338–1347, Oct. 2009.

[9] S. Palaniappan and S. K. Sastry, "Electrical conductivities of selected solid foods during ohmic heating," *J. Food Process Eng.*, vol. 14, no. 3, pp. 221–236, 1991.

[10] J. C. Bischof and X. He, "Thermal stability of proteins," *Ann. New York Acad. Sci.*, vol. 1066, no. 1, pp. 12–33, 2006.

[11] A. Mazzoleni *et al.*, "Conductivity values of tissue culture medium from 20 C to 40 C," *Bioelectromagnetics*, vol. 7, no. 1, pp. 95–99, 1986.

[12] U. Zurbuchen *et al.*, "Determination of the temperature-dependent electric conductivity of liver tissue ex vivo and in vivo: Importance for therapy planning for the radiofrequency ablation of liver tumours," *Int. J. Hyperthermia*, vol. 26, no. 1, pp. 26–33, Feb. 2010.

[13] P. A. Garcia *et al.*, "A numerical investigation of the electric and thermal cell kill distributions in electroporation-based therapies in tissue," *PloS One*, vol. 9, no. 8, 2014, Art. no. e103083.

[14] R. C. Martin, 2nd *et al.*, "Treatment of 200 locally advanced (stage III) pancreatic adenocarcinoma patients with irreversible electroporation: Safety and efficacy," *Ann. Surgery*, vol. 262, no. 3, pp. 486–494, Sep. 2015.

[15] J. J. Wendler *et al.*, "Irreversible electroporation (IRE): Standardization of terminology and reporting criteria for analysis and comparison," *Polish J. Radiol.*, vol. 81, pp. 54–64, 2016.

[16] M. Faroja *et al.*, "Irreversible electroporation ablation: Is all the damage nonthermal?," *Radiology*, vol. 266, no. 2, pp. 462–470, 2013.

[17] G. Narayanan *et al.*, "Vessel patency post irreversible electroporation," *Cardiovascular Interventional Radiol.*, vol. 37, no. 6, pp. 1523–1529, 2014.

[18] M. Lundy *et al.*, "Arterio-Enteric fistula after irreversible electroporation," *Amer. Surgeon*, vol. 85, no. 1, pp. e55–e57, Jan. 2019.

[19] J. D. Kaufman *et al.*, "High-frequency irreversible electroporation using 5,000-V waveforms to create reproducible 2- and 4-cm ablation zones—A laboratory investigation using mechanically perfused liver," *J. Vascular Interventional Radiol.*, vol. 31, no. 1, pp. 162–168.e7, Jan. 2020, doi: 10.1109/j.jvir.2019.05.009.

[20] M. B. Sano *et al.*, "Burst and continuous high frequency irreversible electroporation protocols evaluated in a 3D tumor model," *Phys. Med. Biol.*, vol. 63, no. 13, Jul. 2018, Art. no. 135022.

[21] M. B. Sano *et al.*, "Optimization of a single insertion electrode array for the creation of clinically relevant ablations using high-frequency irreversible electroporation," *Comput. Biol. Med.*, vol. 95, pp. 107–117, Apr. 2018.

[22] M. B. Sano, O. Volotskova, and L. Xing, "Treatment of cancer in vitro using radiation and high frequency bursts of sub-microsecond electrical pulses," *IEEE Trans. Biomed. Eng.*, vol. 65, no. 4, pp. 928–935, Apr. 2018.

[23] M. B. Sano *et al.*, "Asymmetric waveforms decrease lethal thresholds in high frequency irreversible electroporation therapies," *Sci. Rep.*, vol. 7, Jan. 2017. Art. no. 40747.

[24] M. B. Sano *et al.*, "Reduction of muscle contractions during irreversible electroporation therapy using high frequency bursts of alternating polarity pulses: A laboratory investigation in an ex vivo swine model," *J. Vascular Interventional Radiol.*, vol. 29, pp. 893–898, 2017.

[25] M. B. Sano *et al.*, "Production of spherical ablations using nonthermal irreversible electroporation: A laboratory investigation using a single electrode and grounding pad," *J. Vascular Interventional Radiol.*, vol. 27, no. 9, pp. 1432–1440 e3, Sep. 2016.

[26] M. B. Sano *et al.*, "In-vitro bipolar nano- and microsecond electro-pulse bursts for irreversible electroporation therapies," *Bioelectrochemistry*, vol. 100, pp. 69–79, Dec. 2014.

[27] M. B. Sano *et al.*, "Bursts of bipolar microsecond pulses inhibit tumor growth," *Sci. Rep.*, vol. 5, Oct. 2015, Art. no. 14999.

[28] I. A. Siddiqui *et al.*, "High-frequency irreversible electroporation: Safety and efficacy of next-generation irreversible electroporation adjacent to critical hepatic structures," *Surgical Innov.*, vol. 24, no. 3, pp. 276–283, Jun. 2017.

[29] P. A. Garcia *et al.*, "Predictive therapeutic planning for irreversible electroporation treatment of spontaneous malignant glioma," *Med. Phys.*, vol. 44, no. 9, pp. 4968–4980, Sep. 2017.

[30] J. W. Ivey *et al.*, "Targeted cellular ablation based on the morphology of malignant cells," *Sci. Rep.*, vol. 5, Nov. 2015, Art. no. 17157.

[31] T. Miklovic *et al.*, "A comprehensive characterization of parameters affecting high-frequency irreversible electroporation lesions," *Ann. Biomed. Eng.*, vol. 45, no. 11, pp. 2524–2534, Nov. 2017.

[32] T. J. O'Brien *et al.*, "Effects of internal electrode cooling on irreversible electroporation using a perfused organ model," *Int. J. Hyperthermia*, vol. 35, no. 1, pp. 44–55, Jan. 2018.

[33] S. J. Beebe *et al.*, "Induction of cell death mechanisms and apoptosis by nanosecond pulsed electric fields (nsPEFs)," *Cells*, vol. 2, no. 1, pp. 136–162, 2013.

[34] P. Liang *et al.*, "Percutaneous cooled-tip microwave ablation under ultrasound guidance for primary liver cancer: A multicentre analysis of 1363 treatment-naive lesions in 1007 patients in China," *Gut*, vol. 61, no. 7, pp. 1100–1101, 2012.

[35] A. Golberg and M. L. Yarmush, "Nonthermal irreversible electroporation: Fundamentals, applications, and challenges," *IEEE Trans. Biomed. Eng.*, vol. 60, no. 3, pp. 707–714, Mar. 2013.

[36] T. L. Ellis *et al.*, "Nonthermal irreversible electroporation for intracranial surgical applications: Laboratory investigation," *J. Neurosurg.*, vol. 114, no. 3, pp. 681–688, 2011.

[37] P. Garcia *et al.*, "Intracranial nonthermal irreversible electroporation: In vivo analysis," *J. Membrane Biol.*, vol. 236, pp. 127–136, 2010.

[38] A. Rolong *et al.*, "High-frequency irreversible electroporation targets resilient tumor-initiating cells in ovarian cancer," *Integrative Biol. (Cambridge)*, vol. 9, no. 12, pp. 979–987, Dec. 2017.

[39] H. Shafiee *et al.*, "A preliminary study to delineate irreversible electroporation from thermal damage using the arrhenius equation," *J. Biomech. Eng.*, vol. 131, no. 7, 2009, Art. no. 074509.

[40] C. M. Edelblute *et al.*, "Moderate heat application enhances the efficacy of nanosecond pulse stimulation for the treatment of squamous cell carcinoma," *Technol. Cancer Res. Treatment*, vol. 17, 2018, Art. no. 1533033818802305.

[41] F. S. Barnes, "Cell membrane temperature rate sensitivity predicted from the Nernst equation," *Bioelectromagnetics*, vol. 5, no. 1, pp. 113–115, 1984.

[42] M. Kandušer *et al.*, "The temperature effect during pulse application on cell membrane fluidity and permeabilization," *Bioelectrochemistry*, vol. 74, no. 1, pp. 52–57, 2008.

[43] F. de Meyer and B. Smit, "Effect of cholesterol on the structure of a phospholipid bilayer," *Proc. Nat. Acad. Sci.*, vol. 106, no. 10, pp. 3654–3658, 2009.

[44] A. Silve *et al.*, "Comparison of the effects of the repetition rate between microsecond and nanosecond pulses: Electropermeabilization-induced electro-desensitization?," *Biochimica et Biophysica Acta (BBA)-General Subjects*, vol. 1840, no. 7, pp. 2139–2151, 2014.